Title: Novel g-C_3N_4/TiO_2/PAA/PTFE Ultrafiltration Membrane Enabling Enhanced Antifouling and Exceptional Visible-light Photocatalytic Self-cleaning

Authors: Lina Chi, Yingjia Qian, Junqiu Guo, Xinze Wang, Hamidreza Arandiyan, Zheng Jiang

PII: S0920-5861(18)30885-X
DOI: https://doi.org/10.1016/j.cattod.2019.02.027
Reference: CATTOD 11979

To appear in: *Catalysis Today*

Received date: 20 December 2018
Revised date: 7 February 2019
Accepted date: 13 February 2019

Please cite this article as: Chi L, Qian Y, Guo J, Wang X, Arandiyan H, Jiang Z, Novel g-C_3N_4/TiO_2/PAA/PTFE Ultrafiltration Membrane Enabling Enhanced Antifouling and Exceptional Visible-light Photocatalytic Self-cleaning, *Catalysis Today* (2019), https://doi.org/10.1016/j.cattod.2019.02.027

Novel g-C_3N_4/TiO_2/PAA/PTFE Ultrafiltration Membrane Enabling Enhanced Antifouling and Exceptional Visible-light Photocatalytic Self-cleaning

Lina Chi,[a,b]* Yingjia Qian,[a] Junqiu Guo,[b] Xinze Wang,[a] Hamidreza Arandiyan,[c] Zheng Jiang [b]*

[a] *School of Environmental Science and Engineering, Shanghai Jiao Tong University, Shanghai 200240, China*

[b] *Faculty of Engineering and Physical Sciences, University of Southampton, Southampton, SO17 1BJ, UK*

[c] *Laboratory of Advanced Catalysis for Sustainability, School of Chemistry, The University of Sydney, Sydney 2006, Australia*

**Corresponding Authors:*

lnchi@sjtu.edu.cn (L. C) Tel: +86 21-54745361, Z.Jiang@soton.ac.uk(Z. J) Tel: +44 23-80594893

Graphic Abstract

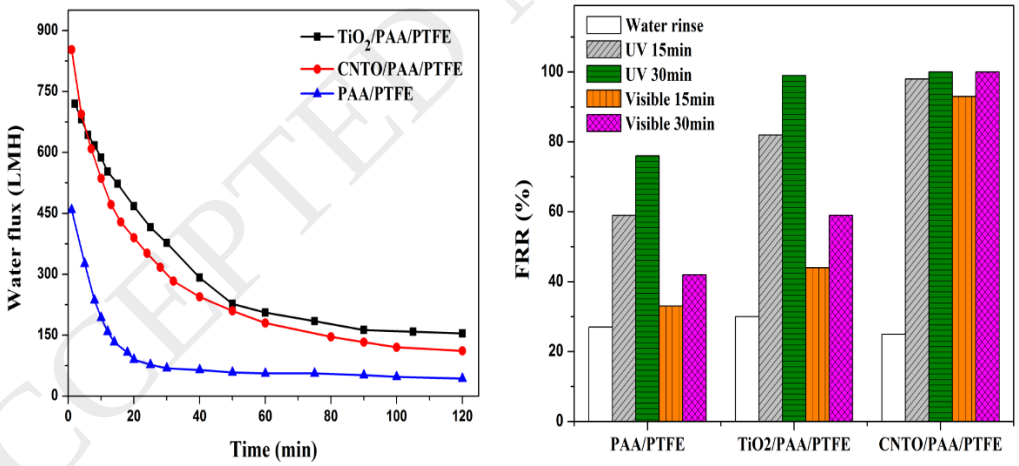

Research Highlights

- The g-C_3N_4/TiO_2 heterojunction nanoparticles are firmly immobilised on PAA/PTFE UFM;
- The g-C_3N_4/TiO_2/PAA/PTFE UFM shows superb hydrophilicity, anti-fouling and water flux;

- Exceptional visible-light regeneration of the fouled g-C_3N_4/TiO_2/PAA/PTFE is demonstrated.
- The enhanced anti-fouling and photocatalytic self-cleaning mechanisms are reasonalised.

Abstract

Membrane fouling due to superhydropobicity of polytetrafluoroethylene ultrafiltration membranes (PTFE UFMs) represents a grand challenge for their practical applications in diverse water treatment industries. Surface immobilisation of hydrophilic and chemically stable inorganic metal oxides (TiO_2, ZrO_2, etc) has been developed to improve hydrophilicity of the PTFE UFMs, though they still suffer from expensive and repeating regenerations once fouled. To address such issues, we strive to firmly immobilize g-C_3N_4 modified TiO_2 (g-C_3N_4/TiO_2, hereafter CNTO) onto PTFE UFM via a facile plasma-enhanced surface graft technique using polyacrylic acid (PAA) as a bridging agent. As reported here, the obtained CNTO/PAA/PTFE UFM shows much smaller surface water contact angle (WCA) of 62.3° than that of bare PTFE UFM(115.8°), leading to enhanced water flux of 830 $L•m^{-2}•h^{-1}$ in the initial ultrafiltration of MB-modelled waste-water. The CNTO/PAA/PTFE UFM is also highly resistant to fouling in the prolonged filtration of 1000 mg/L bovine serum albumin (BSA) solution, while the fouled CNTO/PAA/PTFE UFM is able to regenerate rapidly under either UV or visible-light irradiation. The enhanced performance of the novel CNTO/PAA/PTFE UFM is reasonably attributed to the high wettability and robust photocatalytic activity of the g-C_3N_4/TiO_2 coating that takes different self-cleaning mechanisms under UV and visible light irradiations.

KEYWORDS: PTFE; g-C_3N_4; TiO_2; visible-light photocatalysis; anti-fouling; self-cleaning.

1. Introduction

Porous polytetrafluoroethylene ultrafiltration membrane (PTFE UFM) is one of the most stable and widely applied polymeric UFMs in diverse filtration industrial processes, owing to its superb chemical stability, mechanical strength, anti-erosion and biocompatibility [1, 2]. However, the superhydrophobicity of PTFE often

causes increased bio-fouling and reduced water flux in operation that requires extra energy and costly membrane regeneration [3, 4]. As a viable solution to improve hydrophilicity of PTFE UFM, the surface modification using inorganic metal oxides (MOs) has been extensively explored[5, 6] , for which TiO_2 photocatalyst is redeemed an ideal coating material enabling a hydrophilicity, antifouling and photocatalytic self-cleaning PTFE surface[7-9]. Nevertheless, the tight binding between TiO_2 and polymeric materials is an enormous challenge [10-12] because the intrinsic superhydrophobicity of PTFE prevents inorganic MOs immobilising firmly onto its surface [13-15].

Recently, we established a novel and effective 3-step successive manufacturing protocol for tightly binding TiO_2 layer onto PTFE UFM [16, 17]: First, the strong C-F and C-C bonds of PTFE surface were broken by active plasma to generate free radicals on the membrane surface, which immediately transformed to relatively stable peroxy radicals once exposed to air. In the following second step, as the plasma-treated PTFE immersed into acrylic acid (AA) solution, the peroxy radicals would initiate *in-situ* polymerization of AA to form ultra-thin yet strong bonded poly acrylic acid (PAA) film on PTFE. The tight immobilisation of TiO_2 onto PAA/PTFE was finally realised by sequential dip-coating of TiO_2 sol, because the as-formed PAA layer provided sufficient carboxyl groups as grafting sites to coordinate with Ti cations in strong covalent bonds. In the whole modification process, plasma-grafted PAA acted as a bridge with one end coordinating firmly with TiO_2 and another rooting on the surface of plasma-activated polymers[18-22].

Although the surface TiO_2 functional layer can greatly improve the hydrophilicity and antifouling properties of the PTFE UFMs, their self-cleaning ability can only be realised under energy-intensive UV illumination owing to the large band gap energy (3.2 eV) of TiO_2 [17, 23]. Therefore, it is vital to coat visible-light-responsive TiO_2 on to the PTFE UFMs for better use of the larger portion of the sunlight and thus further reducing operation costs in energy consumption and maintenance[24, 25]. Among various strategies to enhance visible light absorption of TiO_2, combination TiO_2 with a narrow-bandgap semiconductor to form heterojunction is particularly engineering viable because of its operation simplicity and wider possibility. In addition, such heterojunctions can greatly promote charge separation due to built-in electric fields across the interface of

the coupled semiconductors. Among various enabling visible-light photocatalysts, the graphite-like C_3N_4(g-C_3N_4) emerged as a promising semiconductor because of its high stability, small bandgap (~2.7–2.8 eV), appropriate band edges (conduction band minimum and valence band maximum, hereafter CBM and VBM, respectively) [26-28], and desirable photocatalytic activity [24-29].

In the present work, surface modification of porous PTFE membranes by g-C_3N_4/TiO_2 was realised via a plasma-enhanced surface graft of PAA prior to coating g-C_3N_4/TiO_2 layer. The obtained g-C_3N_4/TiO_2/PTFE-UFMs (CNTO/PAA/PTFE) were well characterized using scanning electron microscopy (SEM), X-ray diffraction (XRD), Fourier transform infrared spectroscopy (FTIR), X-ray photoelectron spectroscopy (XPS), and water contact angle measurements. The exceptional anti-fouling and the self-cleaning property of the CNTO/PAA/PTFE UFMs were confirmed by the experiments of ultrafiltration of bovine serum albumin (BSA), photocatalytic removal of MB and photocatalytic regeneration of the fouled UFMs.

2. Experimental

2.1 Materials

Bare PTFE microfiltration membrane (0.5 μm) which uses PET as the substrate and the commercial hydrophilic PTFE membrane were both supplied by Valqua Shanghai Co., Ltd. (China). Melamine, $Ti(OBu)_4$, acetic acid (AA), potassium persulfate, and bovine serum albumin (BSA; Mw = 67,000 Da) were purchased from Sinopharm Chemical Reagent Co., Ltd. (China). The commercial TiO_2 nanoparticle (P25) was supplied by Aladdin Reagent Co., Ltd. Analytical grade acetic acid; nitric acid, absolute ethanol, and ethylene glycol were obtained from Shanghai Lingfeng Chemical Reagent Co., Ltd. (China). All reagents were used without further purification. Distilled water was used throughout the study.

2.2 CNTO composites synthesis

The g-C_3N_4/TiO_2 composite photocatalyst (CNTO) was synthesized by a simple calcination of the mixture of melamine powder with commercial TiO_2 particles. 5.0 g melamine powder was mixed with 2g P25 in the fixed mass ratio of 2.5. The mixture was first combined in beaker and mixed with deionized water with

sufficient stirring and then dried at 60 °C for 1 h to evaporate all the water. The obtained powder was annealed in muffle furnace up to 520 °C for 4 h in a 2 °C min^{-1} heating ramp and cooled to room temperature to get the CNTO composites.

2.3 Membrane modification procedures

A 3-step modification methodology was developed to modify the PTFE membranes, including the successive processes [17].: plasma pre-treatment of PTFE, graft polymerization of AA onto pre-treated PTFE to form PAA/PTFE, and TiO_2 self-assembly onto the PAA/PTFE to obtain the composite membranes. Briefly, plasma (10 sccm) was generated using a CTP-2000 K device (Corona Lab, China) at an excitation frequency of 10 KHz. The clean and dry bare PTFE membranes were placed 8 mm distance from the plasma electrode within the chamber of plasma generator which is filled with flow N_2.

After 120s plasma treatments at discharge power of 60 W, the pre-treated membranes were then exposed to air for 10 min before immersing in an aqueous AA solution for *in-situ* graft PAA polymer. The aqueous AA solution contains 20 wt% AA monomer, 1 wt% potassium persulfate as initiator and the ethylene glycol (EG) as crosslinker (the molar ratio of EG:AA= 1:6.5). The plasma-treated PTFE membrane was immersed in the monomer solution for 5 min and then rolled the residual AA use a clean glass rod for coating PAA evenly. The membrane was then placed between two clean glass plates before drying in a vacuum oven at 75°C for 4 h. The grafting step could form an appropriate layer of PAA on the PTFE membrane surface, which is a crucial step because the coated PAA provides COO^- to functional groups that will coordinate with Ti^{4+} to form a tight TiO_2 coat in the following step.

In the third step, the as-prepared PAA/PTFE membranes were dipped in either 53.5 ml TiO_2 sol or 53.5ml 0.05 wt% CNTO suspended water solution for 20 min, following with before thorough washing and then drying in the oven at 60 °C for 12 hours. The TiO_2/PAA/PFFE and CNTO/PAA/PTFE composite membranes were thus formed. The above mentioned TiO_2 sol was prepared according to our previous work[17].

2.4 Characterizations

The modified PTFE membrane were characterized by the following methods. The surface morphology was observed on a Sirion 200 E scanning electron microscope (SEM) and transmission electron microscope (TEM). The samples were treated by desiccation and sprayed gold before SEM observation. The chemistry nature of the membranes was investigated using a Thermo Fisher Nicolet 6700 Fourier transform infrared (FTIR) spectrometer and Kratos X-ray photoelectron spectroscopy (XPS).

2.4.2 Photocatalytic degradation of MB

Methylene Blue (MB) was used as a model pollutant to preliminarily evaluate the photodegradation ability of CNTO/PAA/PTFE modified membranes under UV light and visible light irradiation, respectively. As for the CNTO/PAA/PTFE modified membranes, the membrane sample with certain area was tailored to unify the TiO_2 loading of 10 mg on the membrane, and then immersed them in 100 mL methylene blue (MB, 10mg/L) aqueous solution in a beaker. The pH of the MB solution was adjusted to neutral (pH=7.0) using dilute sodium hydroxide (NaOH) and chloride acid (HCl). At ambient temperature, the beaker was positioned directly under simulated sunlight irradiation generated from a 500 W Xe lamp (15 cm above the dishes) light source, to which a 400 nm cutoff filter would be mounted to remove UV light. Before light irradiation, the UFMs were suspended in a beaker containing MB solution under magnetic stirring in dark for an hour to establish a MB adsorption–desorption equilibrium on the UFMs. During photocatalysis, a 4 mL reaction solution was taken out every 10 min, filtered and measured using a UV-visible spectrophotometer (Perkinelmer, Lambda 650, USA). For comparison, the photodegradation of MB on bare PTFE membrane was also conducted using the same method.

Since the MB concentration of the aqueous solution was rather low, its photodegradation followed a pseudo-first-order reaction. The kinetic rate equation can be expressed as:

$$-\ln\left(\frac{C}{C_0}\right) = \qquad \text{……..(1)}$$

where k is the apparent rate constant, C_0 the initial MB concentration at adsorption-desorption equilibrium, C the temporal MB concentrations, and t the irradiation duration in minute while sampling.

2.4.3 Membrane filtration performance

The antifouling property of CNTO/PAA/PTFE and TiO_2/PAA/PTFE modified membranes was assessed through filtration experiments conducted in a dead-end filtration cell with a total filtration area of 0.0139 m^2. Under the transmembrane pressure of 100 KPa at room temperature, the accumulated volume of permeation was collected for 15 min after 30 min of pre-operating in terms of LMH ($L•m^{-2}•h^{-1}$). The average water flux (J_{w0}) was calculated through Darcy law:

$$_0 = \frac{}{\Delta} \text{..... .(2)}$$

where V is the permeate volume (L), A the membrane area (m^2), and Δ the permeate time (h).

To investigate fouling property, the sample was fouled in 2 h filtration of the fresh solution of 1 g/L BSA in phosphate buffer saline at pH 7.4. The amount of permeate during filtration was recorded every 30 s using electronic balance, which indicates the decrease of flux during fouling. After continuous filtration of BSA, the pure water flux of the fouled membrane (J_{w1}) was measured to reflect the decrease of filtration capability. The thick protein cake layer left on the membrane surface because protein blocked the pores.

To measure the recovery ability of the membranes, the blocked membranes were cleaned via rinsing with pure water and 15 min and 30 min light irradiation using a 300 W Xe lamp as sunlight simulator. The pure water flux on the recovered membrane (J_{w2}) was then measured to evaluate the performance of the modified membranes. The relative flux recovery ratio (FRR) was calculated using the following equation:

$$\text{FRR} = \frac{_2}{_0} \times 100\% \qquad (3)$$

3. Results

3.1 XRD analysis

Fig. 1 XRD patterns of the bare PTFE and modified PTFE composite membranes.

Fig. 1 shows the XRD patterns of bare PTFE membrane, PAA/PTFE, TiO_2/PAA/PTFE and CNTO/PAA/PTFE composite membranes. In the XRD patterns of the PTFE UFM, the strongest peak at 18.3° can be attributed to the crystalline PTFE and PET while the latter peaks are due to the (100) and (200) diffractions of PET substrate, respectively[30], in accordance with the components of the PTFE/PET UFM. As for the PAA/PTFE UFMs, the shoulder peak at 18.7° is attributed to PAA with low crystallinity overlapped with the diffraction peak of PTFE[31] , meanwhile the PTFE diffraction peak shifts to greater Bragg angle, suggesting the plasma treatment and PAA coating break the PTFE surface C-F bond to form PAA-PTFE composites with different crystalline symmetry from that of PTFE. As either TiO_2 or CNTO coated onto PAA/PTFE, the PTFE diffraction peaks became sharper because of the strong interaction between the inorganic coatings and PAA/PTFE UFMs. The strong interaction between the inorganic coatings and the PTFE/PET UFM is also confirmed by the shifts of PET XRD peaks to smaller Bragg angles.

The loading of TiO_2 can be verified by comparing the XRD patterns between PAA/PTFE and TiO_2/PAA/PTFE UFMs. There are no significant differences between the XRD patterns of TiO_2/PAA/PTFE and CNTO/PAA/PTFE UFMs, because the small loading of C_3N_4 did not change neither the phase nor the

symmetry of the TiO_2 species. In all, the peak shifts of the XRD patterns of these UFMs membranes suggest that the TiO_2 and CNTO composite can be well fixed onto PAA/PTFE UFMs with strong interactions that may be due to the chemical bonds formed between Ti^{4+} and the -COOH of PAA/PTFE substrates. The chemical bonding of the TiO_2 or CNTO to the PAA/PTFE UFMs can be well verified by FTIR spectra [16, 17].

3.2 FT-IR analysis

Fig. 2 shows the FTIR spectra of the PTFE and the modified PTFE membranes. The two strong vibration absorption peaks at 1201 cm^{-1} and 1148 cm^{-1} associated to CF_2 stretching vibrations can be observed on the bare PTFE membrane[32], which become weaker as coated with PAA. On the PAA/PTFE UFM, the weaker PTFE vibrations and a new peak at 1715 cm^{-1}, which is due to C=O bond stretching of carboxyl groups in PAA, suggest the successful graft of PAA onto PTFE via chemical bonds[22].

The FTIR spectra of the TiO_2/PAA/PTFE and CNTO/PAA/PTFE UFMs are completely different from those of PTFE and PAA/PTFE. The vibration peaks due to CF_2 become even weaker after coating with TiO_2 and CNTO upon PAA/PTFE. Meanwhile, strong and broad absorption bands appeared in the region within 500-1100 cm^{-1} may be attributed to the vibrations of Ti-O-Ti and Ti-O bonds in TiO_2 for TiO_2/PAA/PTFE, which are further confirmed by the replacement of carboxyl group vibrations (1715 cm^{-1}) by the carbonate vibrations (1610 ~1360 cm^{-1}). Such IR vibration bands of carbonate species within 1610 ~1520 cm^{-1} and 1440~1360 cm^{-1} for TiO_2/PAA/PTFE reveal the bidentate coordinate binding between Ti cations and carbonyl groups of PAA[16, 17]. In addition, the broad and weak stretching vibration band around 3200 cm^{-1} may be assigned to Ti-OH and surface-adsorbed water[10].

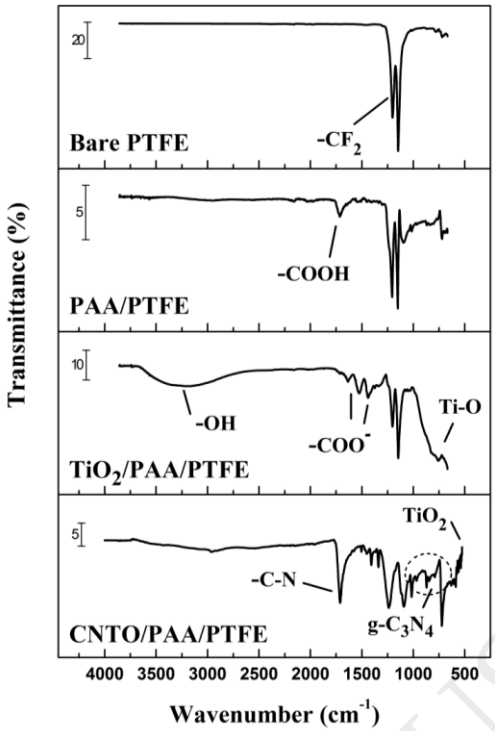

Fig. 2 FT-IR spectra of the PTFE, PAA/PTFE, TiO_2/PAA/PTFE, CNTO/PAA/PTFE UFMs.

More sensitive than XRD, the distinct differences between FTIR spectra (Fig.2) of TiO_2/PAA/PTFE and CNTO/PAA/PTFE UFMs verify that the existence of C_3N_4 in the CNTO/PAA/PTFE: the new multiple peaks in the FTIR bands between 600 and 900 cm^{-1} are due to $-NH_2$ vibrations, and the vibration bands of 1200-1640 cm^{-1} are associated to the typical stretching and rotation vibration of C-N and C=N. The -OH vibration at 3200 cm^{-1} becomes weaker and broader than those peaks of TiO_2/PAA/PTFE because the lower density of surface –OH group on the CNTO than TiO_2.

Furthermore, the frequency difference ($\Delta\nu_t$) between the antisymmetric (ν_{as}, 1610 ~1520 cm^{-1}) and symmetric (ν_s, 1440~1360 cm^{-1}) stretching vibrations for titanium carboxylates can be applied to define the surface COO^--Ti binding nature, by comparing $\Delta\nu_t$ of COO^{-1}-Ti bands with $\Delta\nu_t$ of sodium carbonate[21, 33]. As shown in Table1, the smaller $\Delta\nu_t$ of the TiO_2-based PTFE UFMs than that of Na_2CO_3 reveals the Ti and the surface carbonyl groups on PAA/PTFE UFMs are bidentate coordinated ($\Delta\nu_t < \Delta\nu_0$), which is much stronger than the monodentate ($\Delta\nu_t > \Delta\nu_0$) and bridging bidentate ($\Delta\nu_t \approx \Delta\nu_0$) binding modes[33]. The stronger titanium-carboxylate species are also evidenced by the blue shifts of O 1s and C 1s XPS spectra (see in section 3.3) for the TiO_2/PAA/PTFE and CNTO/PAA/PTFE UFMs relative to those of PAA/PTFE.

Table 1 Vibration frequency of surface carboxylate species

Vibration modes	ν_{as} (COO^--M)/cm^{-1}	ν_{as}(COO^--M)/cm^{-1}	ν_{as}- ν_s/cm^{-1}
COO^--Na	1573	1408	165 (Δ_0)
COO^--TiO_2	1525	1374	151 (Δ)
COO^--CNTO	1505	1407	98 (Δ)

3. 3 XPS analysis

The XPS survey spectra (Fig.3) of the PTFE, PAA/PTFE, TiO_2/PAA/PTFE and the CNTO/PAA/PTFE UFMs. Compared to the XPS survey spectrum of PTFE, the enhanced O 1s XPS signals as well as the reduced C and F XPS signals for the PAA/PTFE reveal PAA was successfully grafted onto PTFE via chemical bonding[16]. Different from the reduced XPS signals of the C 1s (binding energy, B.E, of 292.3 eV) and F 1s (B.E of 687.1 eV) , the O 1s XPS signals (B.E ~ 531.6 eV) are even stronger for the TiO_2/PAA/PTFE and CNTO/PAA/PTFE UFMs, due to the increased surface oxygen moieties from surface TiO_2 and sublayer PAA. The successful coating of TiO_2 for the TiO_2/PAA/PTFE and CNTO/PAA/PTFE UFMs are verified by the Ti XPS signals at ~464.7 eV in their XPS survey spectra, while the unique N 1*s* XPS peaks around 397.8 eV for the CNTO/PAA/PTFE membrane prove that g-C_3N_4 exists in the CNTO/PAA/PTFE UFM.

Fig. 3 XPS survey spectra of bare and the modified PTFE UF membranes

Fig. 4a shows the XPS spectra of C1s of the modified PTFE composite membranes. The two strong peaks

centered at 290.3 eV and 289.8 eV of bare PTFE are assigned to CF_2 and CF bonds[34], though they turn weaker after modifications because of the graft of PAA and immobilisation with inorganic mdofiers (TiO_2 and CNTO). Moreover, in the C1s XPS spectrum of CNTO/PAA/PTFE, the broad peak around 286.0 eV and 282.0 eV can be well fitted into several absorption peaks, ascribed to C=N at 286.9 eV, C-N at 286.3 eV, C=O at 286.4 eV, and Ti-C at 282.6 eV[35]. Fig.4b comparatively shows the O1s core level XPS spectra of TiO_2/PAA/PTFE and CNTO/ PAA/PTFE, in which the binding energies of 531.2 eV can be ascribed to the hydroxyl radicals and carbonyl group while the peak at 529.9 eV is assigned to the lattice oxygen of TiO_2[36].

Fig. 4 The core level (a) C1s and (b) O1s XPS spectra of bare and modified PTFE UFMs, (c) N1s and (d) Ti2p XPS spectra of CNTO/PAA/PTFE UFM.

The asymmetrical N1s XPS spectrum (Fig. 5c) of the CNTO/PAA/PTFE UFM suggest the co-existence of a number of distinguishable nitrogen environments: the peak at 398.1 ev and 399.9 eV are due to the N=C atoms bonds in sp^2 modes and the N-$(C)_3$ group in sp^3 coordination, respectively. Ti 2p XPS spectra of

TiO_2/PAA/PTFE and CNTO/PAA/PTFE UFMs (Fig. 5d) are attributed to the Ti $2p_{1/2}$ (462.8 eV) and Ti $2p_{3/2}$ (457.2 eV) with the binding energy split of 5.7 eV[36].

3.4 SEM analysis

The surface morphology evolution of PTFE membranes with respect to the modification process was investigated by SEM and the obtained images of the membranes are shown in Fig.5. Fig.5a shows the SEM image of the bare PTFE membrane which is composed of uniform microfibers (diameter of 0.5 μm) interweaven to form multi-scale micropores. The SEM image of the PAA/PTFE (Fig.5b) reveals that the plasma-treatment and surface graft of PAA don't change the fibrous morphology of PTFE but significantly change the surface roughness.

The PTFE fibers cannot be observed in the SEM images of TiO_2/PAA/PTFE (Fig.5c) and CNTO/PAA/PTFE (Fig.5d) because the PAA/PTFE fibres are well masked by the TiO_2 and CNTO inorganic coatings. The high resolution SEM image of the TiO_2/PAA/PTFE (Fig.5e) suggests that amorphous TiO_2 has been well coated on PAA/PTFE UFM though sub-micrometre TiO_2 particles (diameter in ~0.3 μm) and their aggregates are randomly anchored on the TiO_2 coating. However, the closer SEM observation of CNTO/PAA/PTFE (Fig.5f) shows CNTO aggregates on the PAA/PTFE fibres in smaller nano-particles without continuous amorphous TiO_2 coating. Although the immobilised CNTO aggregates possess greater sizes than the TiO_2 islands of TiO_2/PAA/PTFE, such hierarchical CNTO particles are comprised of smaller nano-particles of TiO_2 and C_3N_4. The mixture of C_3N_4/TiO_2 would lead to enhanced photocatalytic active surface (see section 3.6), whereas the lower coverage of CNTO on PAA/PTFE fibres might cause lower wettability of CNTO/PAA/PTFE than that of TiO_2/PAA/PTFE. Therefore, one can imagine that these PTFE-based UFMs would display distinct surface properties due to their different surface components and morphologies.

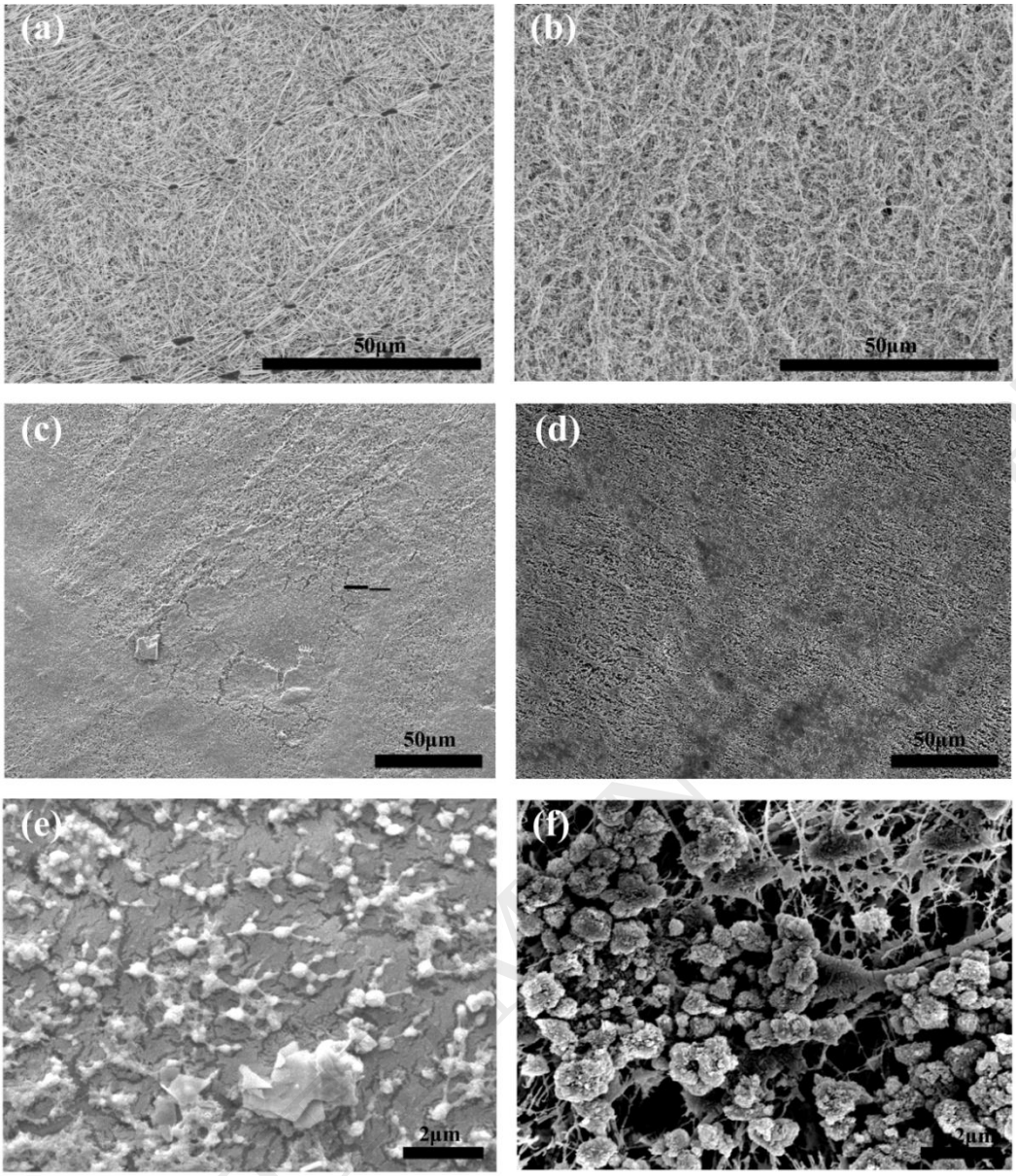

Fig. 5 SEM images of Bare PTFE (a), PAA/PTFE (b), TiO_2/PAA/PTFE (c), CNTO/PAA/PTFE(d), and high-resolution SEM images of the TiO_2/PAA/PTFE (e) and CNTO/PAA/PTFE(f).

3.5 Surface hydrophilicity

The surface wettability is a crucial factor determining the performance of ultrafiltration membranes and the excellent hydrophilicity is desired for high water flux for ultrafiltration. Herein, the sessile drop method was adopted to measure the water contact angle (CA) on the PTFE-based UFMs and to index their surface hydrophilicity. As shown in Fig.6a, the CA of PAA/PTFE decreases to 81.9 º as compared to 115.8 ° of PTFE UFM, which is due to the relatively higher hydrophilicity of PAA than PTFE. Now that the inorganic TiO_2

and CNTO materials are more hydrophilic than PAA, the contact angles further decrease to 35.0° and 62.3° once the PAA/PTFE UFMs are coated with TiO_2 and CNTO, respectively. In addition, the exposure of PTFE fibres and the larger roughness of CNTO/PAA/PTFE are responsible for higher CA than that of TiO_2/PAA/PTFE. The evolution of water contact angles during PTFE UFMs modification clearly verify that our modification strategy can effectively promote the surface hydrophilicity of the PTFE UFMs.

Indeed, the steady state (after initial 20 minutes) water flux of the modified PTFE UFMs are improved dramatically as compared to the zero flux of hydrophobic bare PTFE membranes. As indicated in Fig.6b, the water flux of CNTO/PAA/PTFE UFM is ~822.86 $L•m^{-2}•h^{-1}$, comparable to that (848.57 $L•m^{-2}•h^{-1}$) of TiO_2/PAA/PTFE. More importantly, the hydrophilic CNTO and TiO_2 coatings are very stable, without significant water flux reduction after 60-hour stability tests under rigorous stirring.

Fig. 6 The water contact angle (a) and water flux (b) of the bare and modified PTFE UFMs

3.6 Photocatalytic activity and stability

Methylene Blue (MB) was used as a model compound to investigate the photocatalytic self-cleaning ability of TiO_2/PAA/PTFE and CNTO/PAA/PTFE UFMs under UV-vis irradiation using a 500 w Xe lamp. As shown in Fig. 7a, after 100 min UV-vis illumination, the approximately 5% MB removal rate is achieved on the bared PTFE membrane, owing to the UV-initiated photodegradation of MB, though the MB removal rates achieve 90% and 82% on the CNTO/PAA/PTFE and TiO_2/PAA/PTFE UFMs, respectively. The enhanced MB removals can be well assigned to the excellent photocatalytic activity of CNTO and TiO_2. The slightly

higher photocatalytic MB removal ability on the CNTO/PAA/PTFE than that on TiO_2/PAA/PTFE are due to the fact that CNTO is responsive to both UV and visible light but TiO_2 solely responses to UV.

Fig. 7 MB photodegradation on the bare and modified PTFE UFMs under UV-vis (a) and visible light (b)

Fig. 8 The cycling tests of MB photodegradation performance on the CNTO/PAA/PTFE UFM

As shown in Fig. 7b, under visible light irradiation (λ>400 nm) for 100 minutes, the MB removal achieves 78% on the CNTO/PAA/PTFE, much higher than the 40% MB removal rate of the TiO_2/PAA/PTFE. The former is due to the visible-light photocatalytic degradation of MB while the latter is due to the MB dye-sensitised photocatalytic effects. It is worth noting that due to higher coverage and specific surface area (SSA=134.5 m^2/g) of the TiO_2, TiO_2/PAA/PTFE membranes exhibits higher equilibrium adsorption capacity

of MB than those of PTFE and CNTO/PAA/PTFE of which the SSA is 89 m^2/g. Although the SSA and equilibrium adsorption of CNTO/PAA/PTFE are relatively lower than TiO_2/PAA/PTFE, its shows superb photocatalytic activity, which may be assigned to the synergy of the visible-light response of CNTO, the dye sensitisation effects and the enhanced charge carrier separation due to the staggered heterojunction between g-C_3N_4 and TiO_2 (as discussed in section 4). Moreover, the high MB photodegradation activity on CNTO/PAA/PTFE remains in the multi-cycle tests (Fig.8) although they are slightly declined than the fist test, verifying its excellent stability and great promise as a self-cleaning UFM for wastewater purification practice. The slight decline of decolorisation activity is induced by the incomplete mineralisation of organic species in the previous cycling tests runs.

3.7 Antifouling and photocatalytic regeneration

Fig. 9 Time-dependent water flux of the modified PTFE UFMs in ultrafiltration of 1g/L BSA at 0.1MPa (a) and the flux recovery ratios of the modified PTFE UFMs washed with different methods.

Fig.9a shows the water fluxes of the PAA/PTFE, TiO_2/PAA/PTFE, and CNTO/PAA/PTFE UFMs for continuous filtration of BSA (1000 ppm) solution. The water flux of the PAA/PTFE declines ~80% after 20 min continuous ultrafiltration operation, whereas the water fluxes decline much more slowly for the TiO_2/PAA/PTFE and CNTO/PAA/PTFE UFMs. The protein retention rates, which is another important index for UFMs, achieve ~72% of TiO_2/PAA/PTFE, and CNTO/PAA/PTFE UFMs in the steady filtrations, revealing their excellence antifouling property. However, water fluxes of TiO_2/PAA/PTFE and

CNTO/PAA/PTFE decrease remarkably after 120 minute continuous operation in such an accelerated fouling tests. The declined water flux is due to the accumulated fouling which requires membrane regeneration.

The recovery of water flux by washing is vital to assess the reliability of the UFMs for the practical applications of UFMs, while the UFM washing is energy and environment unfriendly process. Herein, water flux recovery of the BSA-fouled UFMs is compared after water resining and photocatalytic resining under UV and visible light illumination, respectively, so as to assess the effectiveness of photocatalyst modification. As shown in Fig. 9b, the PAA/PTFE, TiO_2/PAA/PTFE and CNTO/PAA/PTFE UFMs displayed comparable water flux after direct water resining without light assistance, though illuminating by UV-vis light can greatly enhanced water flux recovery ability for the photocatalyst modified UFMs, suggesting that photocatalysis can significantly facilitate regeneration of fouled UFMs.

e quantitative comparison of the flux recovery ratio (FRR, listed in Table 2) indicates that water flux on the washed TiO_2/PAA/PTFE and CNTO/PAA/PTFE UFMs recovered 82% and 98% after 15-min UV exposure, approximately 1.5 times that of PAA/PTFE (59%). Further UV exposure up to 30-min can completely recover the water fluxes of the fouled TiO_2/PAA/PTFE and CNTO/PAA/PTFE UFMs. The results confirm the core roles of the photocatalysts for self-cleaning, because the water flux of the fouled PAA/PTFE cannot be fully recovered in 30-min UV illumination although UV illumination itself can promote regeneration. It is also notable that the CNTO/PAA/PTFE exhibited superior water flux to TiO_2/PAA/PTFE in the 15-min UV regeneration process, which is mainly attributed to the improved separation of charge carrier on the C_3N_4-TiO_2 than TiO_2 because they both are responsive to UV.

Table 2 Antifouling performances of the modified PTFE membranes.

Membranes	FRR (%)				
	Water rinsing	UV/15 min	UV/30 min	Visible/15 min	Visible/30 min
PAA/PTFE	26	59	76	33	42
TiO_2/PAA/PTFE	30	82	99	44	59
CNTO/PAA/PTFE	25	98	100	93	100

Under visible-light (>400 nm) irradiation, the flux recovery ability of the CNTO/PAA/PTFE is much higher than those of PAA/PTFE and TiO_2/PAA/PTFE. Under visible-light irradiation, the negligible time-dependent increments of FRR on the PAA/PTFE and the TiO_2/PAA/PTFE UFM suggest the adsorbed BSA is hard to remove and visible-light is not effective for these UFMs. However, the CNTO/PAA/PTFE displays excellent recovery rate of the FRR, achieving 93% and 100% after 15 and 30 min of visible light irradiation, respectively. Apparently, the visible-light-responsive regeneration ability of CNTO/PAA/PTFE is comparable to that induced by UV irradiation. Because the non-photocatalytic water-resining regeneration ability of CNTO/PAA/PTFE is lower than that of TiO_2/PAA/PTFE, the superior FRR of CNTO/PAA/PTFE under irradiations should be dominated by the photocatalytic self-cleaning effects of CNTO coating.

4. Discussion

The above experimental results suggest that the superior self-cleaning and photocatalytic regeneration on the CNTO/PAA/PTFE to those of TiO_2/PAA/PTFE UFM under both UV and visible-light are arisen from the enhanced the photocatalysis on the CNTO coating. The recent research and review articles indicated that the photocatalytic performance of semiconductor materials highly depends on their band structures, including bandgap and band edges[37-40], because the bandgap energy (Eg) determines the light absorption while the band edges determine the activities of the photogenerated charge carriers[37, 38, 40]. In order to unravel the mechanistic origination of the self-cleaning and enhanced regeneration ability, the band structures of the coated CNTO materials is analysed, which is peculiarly important for understanding its excellent visible-light regeneration performance.

4.1 Energy band diagrams of CNTO

The Mulliken electronegativity methodology, which was proved adequate and has been widely applied [24-27, 29, 37, 41-44], was adopted to estimate the band structure of the CNTO composite. The band edge potentials can be estimated by inserting the experimental Eg values of C_3N_4 (2.75 eV) and TiO_2 (3.2 eV) and the compound

electronegativity values into the following empirical equations [41-44]:

$E_{VBM} = X - E^e + 0.5Eg$ ……(4)

$E_{CBM} = E_{VBM} - Eg$ ……(5)

Where E_{VBM} and E_{CBM} are the potentials of the VB and VB edge, X the electronegativity of the semiconductor compounds (4.72 eV for g-C_3N_4, 5.81 eV for TiO_2), E^e the free electron energy of standard hydrogen electrode (SHE at pH=0, 4.5 eV versus vacuum). Fig. 10 illustrates the calculated VBM and CBM potentials of g-C_3N_4 and TiO_2 in the SHE scale, 1.60 eV and -1.15 eV of g-C_3N_4, 2.91 eV and -0.29 eV for TiO_2, respectively. Because g-C_3N_4 and TiO_2 are combined intimately in CNTO as proved by SEM (Fig. 5), they should form a staggered heterojunction in terms of their band edge alignment (Fig. 10).

4.2 Mechanism of visible-light-driven photocatalytic self-cleaning on CNTO/PAA/PTFE

Under the visible light irradiation (>400 nm) of our CNTO/PAA/PTFE, as shown in Fig.10a, its g-C_3N_4 can be excited to generate e^- and h^+ for photocatalytic self-cleaning rather than the TiO_2 constituent. which also interprets why TiO_2/PAA/PTFE cannot display enhanced FRR under visible-light regeneration (Table 2) despite the fact that it is active in MB photodegradation (Fig.7b). The slightly higher FRR TiO_2/PAA/PTFE than PAA/PTFE would be due to the intrinsically higher hydrophilicity of TiO_2 than PAA and PTFE.

Fig.10 The proposed photocatalytic self-cleaning mechanism of CNTO/PAA/PTFE under visible light (a), under UV light (b)

Furthermore, on the CNTO/PAA/PTFE, the photogenerated h^+ (~1.60 eV) of g-C_3N_4 is energetically adequate to break down the adsorbed pollutants, meanwhile the photogenerated e^- at CBM (-1.15 eV) of excited g-C_3N_4 can be transferred to TiO_2 CBM (-0.29 eV), and then react with dissolved O_2 to generate active $\cdot O_2^-$ species for oxidising surface adsorbed MB and BSA. It is worth stressing that TiO_2 cannot photogenerate e^- and h^+ under visible-light for oxidising pollutant, however it has no VBM h^+ to accept and recombine with the CBM e^- either, so that the TiO_2 serves as e^- capture to cause enhanced separation and reduced recombination of photogenerated charge carriers.

In order to confirm the roles of TiO_2 and g-C_3N_4 in the CNTO/PAA/PTFE, visble-light (400 nm) laser exicited PL spectra of the bare TiO_2, bare g-C_3N_4 and g-C_3N_4/TiO_2 hybrid materials are collected and displayed in Fig.11(a). The strong emission peak centred at about 450 nm for the bare g-C_3N_4 sample, which was similar to the literatures, while PL maxima at 450 nm (3.22eV) and 468 nm of the bare TiO_2 photocatalyst are negligible. For g-C_3N_4/TiO_2 hybrid materials, the position of the emission peak in the PL spectrum was similar to that of the bare g-C_3N_4, but the emission intensity significantly decreased, verifying the recombination of photogenerated charge carriers was greatly inhibited by such donor-acceptor electron transfer. Therefore, under visible light condition, both the e^- at TiO_2 CBM and h^+ at VBM of g-C_3N_4 endowed CNTO/PAA/PTFE UFM with the superior photocatalytic activity and self-cleaning/regeneration ability under visible light irradiation, which is hard to achieve for to TiO_2/PAA/PTFE UFM.

Fig. 11 PL spectra of CNTO composites, as-prepared g-C_3N_4 and TiO_2 under excitation wavelength 400nm (a) and under excitation wavelength 350nm (b)

4.3 Mechanism of UV-driven photocatalytic self-cleaning on CNTO/PAA/PTFE

Under UV irradiation, the photocatalytic self-cleaning of UFMs follows different mechanism from the above visible light photocatalysis process (Fig.10b). For PAA/PTFE, the UV itself can break down both MB and surface adsorbed BSA, so that enhance water flux during the UV-assisted waster resining. The intrinsic contribution of UV to self-cleaning is also existing on the TiO_2/PAA/PTFE and CNTO/PAA/PTFE UFMs, though the photocatalysts play the core roles for self-cleaning.

When the ultrafiltration on TiO_2/PAA/PTFE occurs under UV irradiation, the UV can excite TiO_2 to generate e^- and h^+ of sufficient redox potentials to decompose MB and BSA, resulting much faster MB photodegradation and enhanced water flux. Meanwhile, the UV irradiation also promotes the concentration of–OH groups on TiO_2 surface of TiO_2/PAA/PTFE UFM, leading to higher wettability and water flux as well as extended lifetime in the UF time on stream of BSA.

On the CNTO/PAA/PTFE, the UV-light can excite both g-C_3N_4 and TiO_2. Similar to that on visible-light photocatalysis, the photogenerated e^- of g-C_3N_4 will flow from its CBM to TiO_2 CBM, on which it also hosts UV-exited photogenerated e^- from TiO_2 VBM. Meanwhile, the photogenerated h^+ from TiO_2 VBM will transfer to g-C_3N_4 VBM, leading to more holes available on g-C_3N_4 VBM. Such charge carrier transportation is driven by the built-in electric fields existing in the CNTO heterojunction. Thereby, the e^- density on TiO_2 CBM and h^+ density on g-C_3N_4 VBM are both improved, causing enhanced photocatalytic MB degradation (Fig. 7a) and BSA decomposition (higher water flux after regeneration Table 2).

Because the e^- and h^+ on CNTO/PAA/PTFE and TiO_2/PAA/PTFE UFM are in sufficient redox potentials to break down surface pollutants, the photocatalytic self-cleaning behaviour should be influenced by photocatalytic kinetics and concentration of dissolved oxygen. Indeed, in terms of the regeneration rate, the faster photocatalytic recoveries of water flux in initial 15 minutes than those at steady states (15~30 mins) are observed on the two photocatalyst-modified UFMs (Table 2). Such fast initial kinetics is due to the

regeneration reaction rapidly consumes the dissolved O_2 in solution and decomposes surface-adsorbed organics. The detailed study of the kinetic-influence on the self-cleaning mechanism is ongoing.

As shown in Fig.11b, the PL spectrum of bare TiO_2 photocatalyst shows a broad PL maximum around 385 nm (3.22eV) and a weak maximum at approximatelyt450 nm. The former corresponds to recombination of photo-induced band-gap electrons and holes and the second one is likely caused by midgap recombination of electron and holes due to impurity or structural defects. The bare g-C_3N_4 photocatalyst displays one intensive broad PL band at 450 nm (2.75 eV) due to the bandgap transition of electrons between antibonding π* and bonding π states as well as between the π* and the defect states. For the TiO_2/g-C_3N_4 photocatalyst, its PL is very weak, which can be assigned to the effective separation of charge carriers due to the built-in electric field within the staggered heterojunction.

4.4 Origin of enhanced surface wettability of TiO_2/PAA/PTFE and CNTO/PAA/PTFE

The enhanced wettability of the TiO_2/PAA/PTFE UFM should be attributed to the intrinsic hydrophilicity of the inorganic semiconductor coatings, which was ever discussed elsewhere in detail [16, 17]. The slightly weaker wettability of CNTO/PAA/PTFE relative to TiO_2/PAA/PTFE UFM may be attributed to the hierarchical architectures and the lower hydrophilicity of C_3N_4 than TiO_2.

5. Conclusion

In this article, the CNTO composite was firmly coated onto PAA/PTFE UFM in which the PAA was immobilised via plasma-induced graft of PAA precursor following with *ex-situ* polymerisation on PTFE UFM. The CNTO/PAA/PTFE UFM displayed small water contact angle of 62.3°, which is slightly greater than that of TiO_2/PAA/PTFE UFM (35.0°) but much smaller than that of PTFE (115.8 °). The enhanced wettability of the modified PTFE UFMs led to enhanced water fluxes, 848.6 and 822.9 $L•m^{-2}•h^{-1}$ on the CNTO/PAA/PTFE and TiO_2/PAA/PTFE UFMs, respectively. In the continuous ultrafiltration of BSA solution, the CNTO/PAA/PTFE and TiO_2/PAA/PTFE UFMs respectively remain 200 and 250 $L•m^{-2}•h^{-1}$ water

fluxes in the 120-minute UF operations, much longer than that of PAA/PTFE (~ 60 $L•m^{-2}•h^{-1}$ in only 20-minute ultrafiltration). The improved wettability, longer lifetime (6-times at least) and stabilised water flux of the modified PAA/PTFE are reasonably assigned to intrinsic hydrophilicity of the coated CNTO and TiO_2.

The water flux of the fouled CNTO/PAA/PTFE can be fully recovered after 30 minute regeneration treatments under either UV-vis or visible light, though TiO_2/PAA/PTFE UFM can only be fully regenerated by UV irradiation. The water flux recovery rate under visible-light of the fouled CNTO/PAA/PTFE is comparable to that under UV through different mechanisms: Under visible light (>400 nm) irradiation, the photocatalytic regeneration is governed by the photogenerated h^+ at C_3N_4 VBM and e^- at TiO_2 CBM, in which serves as electron capture/reservoir yet contribution of its VBM is negligible. Under UV, the photogenerated h^+ at C_3N_4 VBM and e^- at TiO_2 CBM determine photocatalytic self-cleaning. Although their e^- and h^+ are in higher density because generated from both C_3N_4 and TiO_2, the rate cap is influenced by the kinetics of the dissolved O_2 and diffusion of interface pollutant.

In all, we provide an effective method for manufacturing CNTO/PAA/PTFE UFM with unprecedented high-performance and promise for practical UF. The excellent ultrafiltration and photocatalytic self-cleaning of CNTO/PAA/PTFE are due to intrinsic hydrophilicity and photocatalytic property of CNTO.

Acknowledgement

We acknowledge the financial supports from the National Key Project on Prevention and Control of Water Pollution from Ministry of Ecology and Environment, China (2017ZX07203-005), the State Key Program of National Natural Science Foundation of China (21737002) and the UK Newton Funds for International Research Collaborations (NRCP/1415/261 and IE160277). JG appreciate the Eustice studentship from the University of Southampton, U.K.

References

[1] H. Chen, Q. Lin, Q. Xu, Y. Yang, Z.P. Shao, Y. Wang, Plasma activation and atomic layer deposition of TiO2 on polypropylene membranes for improved performances of lithium-ion batteries, J. Membr. Sci., 458 (2014) 217-224.

[2] Z.Q. Dong, X.H. Ma, Z.L. Xu, W.T. You, F.B. Li, Superhydrophobic PVDF-PTFE electrospun nanofibrous membranes for desalination by vacuum membrane distillation, Desalination, 347 (2014) 175-183.
[3] S. Bamperng, T. Suwannachart, S. Atchariyawut, R. Jiraratananon, Ozonation of dye wastewater by membrane contactor using PVDF and PTFE membranes, Sep. Purif. Technol., 72 (2010) 186-193.
[4] C.V. Amanchukwu, J.R. Harding, Y. Shao-Horn, P.T. Hammond, Understanding the Chemical Stability of Polymers for Lithium-Air Batteries, Chem. Mat., 27 (2015) 550-561.
[5] N. Peng, N. Widjojo, P. Sukitpaneenit, M.M. Teoh, G.G. Lipscomb, T.S. Chung, J.Y. Lai, Evolution of polymeric hollow fibers as sustainable technologies: Past, present, and future, Prog. Polym. Sci., 37 (2012) 1401-1424.
[6] H.L. Tang, M. Pan, S.P. Jiang, X. Wang, Y.Z. Ruan, Fabrication and characterization of PFSI/ePTFE composite proton exchange membranes of polymer electrolyte fuel cells, Electrochim. Acta, 52 (2007) 5304-5311.
[7] K. Fischer, M. Grimm, J. Meyers, C. Dietrich, R. Glaser, A. Schulze, Photoactive microfiltration membranes via directed synthesis of TiO2 nanoparticles on the polymer surface for removal of drugs from water, Journal of Membrane Science, 478 (2015) 49-57.
[8] L. Frunza, L. Diamandescu, I. Zgura, S. Frunza, C.P. Ganea, C.C. Negrila, M. Enculescu, M. Birzu, Photocatalytic activity of wool fabrics deposited at low temperature with ZnO or TiO2 nanoparticles: Methylene blue degradation as a test reaction, Catalysis Today, 306 (2018) 251-259.
[9] A.-G. Rincón, C. Pulgarin, Bactericidal action of illuminated TiO2 on pure Escherichia coli and natural bacterial consortia: post-irradiation events in the dark and assessment of the effective disinfection time, Applied Catalysis B: Environmental, 49 (2004) 99-112.
[10] S.J. You, G.U. Semblante, S.C. Lu, R.A. Damodar, T.C. Wei, Evaluation of the antifouling and photocatalytic properties of poly(vinylidene fluoride) plasma-grafted poly(acrylic acid) membrane with self-assembled TiO2, J. Hazard. Mater., 237 (2012) 10-19.
[11] S.H.N. Lim, D.G. McCulloch, M.M.M. Bilek, D.R. McKenzie, J. du Plessis, M.V. Swain, R. Wuhrer, The effect of plasma immersion ion implantation on the contact pressure and composition of titanium nitride thin films, Surface and Coatings Technology, 201 (2006) 396-400.
[12] Y. Mansourpanah, S.S. Madaeni, A. Rahimpour, A. Farhadian, A.H. Taheri, Formation of appropriate sites on nanofiltration membrane surface for binding TiO2 photo-catalyst: Performance, characterization and fouling-resistant capability, Journal of Membrane Science, 330 (2009) 297-306.
[13] C.H. Yu, I. Kusumawardhana, J.Y. Lai, Y.L. Liu, PTFE/polyamide thin-film composite membranes using PTFE films modified with ethylene diamine polymer and interfacial polymerization: Preparation and pervaporation application, J. Colloid Interface Sci., 336 (2009) 260-267.
[14] A.G. Lin, S.A. Shao, H.Z. Li, D.Y. Yang, Y. Kong, Preparation and characterization of a new negatively charged polytetrafluoroethylene membrane for treating oilfield wastewater, Journal of

Membrane Science, 371 (2011) 286-292.
[15] Q. Xu, Y. Yang, X.Z. Wang, Z.H. Wang, W.Q. Jin, J. Huang, Y. Wang, Atomic layer deposition of alumina on porous polytetrafluoroethylene membranes for enhanced hydrophilicity and separation performances, Journal of Membrane Science, 415 (2012) 435-443.
[16] Y. Qian, L. Chi, W. Zhou, Z. Yu, Z. Zhang, Z. Zhang, J. Zheng, Fabrication of TiO 2 - modified polytetrafluoroethylene ultrafiltration membranes via plasma-enhanced surface graft pretreatment, Applied Surface Science, 360 (2016) 749-757.
[17] L.N. Chi, Y.J. Qian, B.Y. Zhang, Z.J. Zhang, Z. Jiang, Surface engineering and self-cleaning properties of the novel TiO2/PAA/PTFE ultrafiltration membranes, Appl. Petrochem. Res., 6 (2016) 225-233.
[18] U. Konig, M. Nitschke, A. Menning, G. Eberth, M. Pilz, C. Arnhold, F. Simon, G. Adam, C. Werner, Durable surface modification of poly(tetrafluoroethylene) by low pressure H2O plasma treatment followed by acrylic acid graft polymerization, Colloid Surf. B-Biointerfaces, 24 (2002) 63-71.
[19] C. Wang, J.R. Chen, Studies on surface graft polymerization of acrylic acid onto PTFE film by remote argon plasma initiation, Applied Surface Science, 253 (2007) 4599-4606.
[20] J.P. Chen, Y.P. Chiang, Surface modification of non-woven fabric by DC pulsed plasma treatment and graft polymerization with acrylic acid, Journal of Membrane Science, 270 (2006) 212-220.
[21] B. Hojjati, R.H. Sui, P.A. Charpentier, Synthesis of TiO2/PAA nanocomposite by RAFT polymerization, Polymer, 48 (2007) 5850-5858.
[22] S.S. Madaeni, S. Zinadini, V. Vatanpour, A new approach to improve antifouling property of PVDF membrane using in situ polymerization of PAA functionalized TiO2 nanoparticles, Journal of Membrane Science, 380 (2011) 155-162.
[23] A. Soklic, M. Tasbihi, M. Kete, U.L. Stangar, Deposition and possible influence of a self-cleaning thin TiO2/SiO2 film on a photovoltaic module efficiency, Catalysis Today, 252 (2015) 54-60.
[24] I. Papailias, N. Todorova, T. Giannakopoulou, J.G. Yu, D. Dimotikali, C. Trapalis, Photocatalytic activity of modified g-C3N4/TiO2 nanocomposites for NOx removal, Catalysis Today, 280 (2017) 37-44.
[25] H. Wei, W.A. McMaster, J.Z.Y. Tan, L. Cao, D.H. Chen, R.A. Caruso, Mesoporous TiO2/g-C3N4 Microspheres with Enhanced Visible-Light Photocatalytic Activity, J. Phys. Chem. C, 121 (2017) 22114-22122.
[26] Y. Tan, Z. Shu, J. Zhou, T. Li, W. Wang, Z. Zhao, One-step synthesis of nanostructured g-C3N4/TiO2 composite for highly enhanced visible-light photocatalytic H2 evolution, Applied Catalysis B: Environmental, 230 (2018) 260-268.
[27] F. Chang, J. Zhang, Y.C. Xie, J. Chen, C.L. Li, J. Wang, J.R. Luo, B.Q. Deng, X.F. Hu, Fabrication, characterization, and photocatalytic performance of exfoliated g-C3N4-TiO2 hybrids, Applied Surface Science, 311 (2014) 574-581.

[28] L.C. Wu, H. Zhao, L.G. Jin, H.Y. Xu, TiO2/g-C3N4 heterojunctions: In situ fabrication mechanism and enhanced photocatalytic activity, Front. Mater. Sci., 10 (2016) 310-319.
[29] Q. Zhang, X. Quan, H. Wang, S. Chen, Y. Su, Z.L. Li, Constructing a visible-light-driven photocatalytic membrane by g-C3N4 quantum dots and TiO2 nanotube array for enhanced water treatment, Scientific Reports, 7 (2017) 7.
[30] S. Fernandez, A. Martinez-Steele, J.J. Gandia, F.B. Naranjo, Radio frequency sputter deposition of high-quality conductive and transparent ZnO: Al films on polymer substrates for thin film solar cells applications, Thin Solid Films, 517 (2009) 3152-3156.
[31] S. Bekin, S. Sarmad, K. Gürkan, G. Keçeli, G. Gürdağ, Synthesis, characterization and bending behavior of electroresponsive sodium alginate/poly(acrylic acid) interpenetrating network films under an electric field stimulus, Sensors and Actuators B: Chemical, 202 (2014) 878-892.
[32] J.Y. Qiu, J.F. Ni, M.L. Zhai, J. Peng, H.H. Zhou, J.Q. Li, G.S. Wei, Radiation grafting of styrene and maleic anhydride onto PTFE membranes and sequent sulfonation for applications of vanadium redox battery, Radiat. Phys. Chem., 76 (2007) 1703-1707.
[33] M. Nara, H. Morii, M. Tanokura, Coordination to divalent cations by calcium-binding proteins studied by FTIR spectroscopy, Biochim. Biophys. Acta-Biomembr., 1828 (2013) 2319-2327.
[34] A. Vesel, M. Mozetic, A. Zalar, XPS characterization of PTFE after treatment with RF oxygen and nitrogen plasma, Surf. Interface Anal., 40 (2008) 661-663.
[35] N. Vandencasteele, H. Fairbrother, F. Reniers, Selected effect of the ions and the neutrals in the plasma treatment of PTFE surfaces: An OES-AFM-Contact angle and XPS study, Plasma Process. Polym., 2 (2005) 493-500.
[36] J.D. Andrade, X-ray Photoelectron Spectroscopy (XPS), in: J.D. Andrade (Ed.) Surface and Interfacial Aspects of Biomedical Polymers: Volume 1 Surface Chemistry and Physics, Springer US, Boston, MA, 1985, pp. 105-195.
[37] J. Guo, X. Liao, M.-H. Lee, G. Hyett, C.-C. Huang, D.W. Hewak, S. Mailis, W. Zhou, Z. Jiang, Experimental and DFT insights of the Zn-doping effects on the visible-light photocatalytic water splitting and dye decomposition over Zn-doped BiOBr photocatalysts, Applied Catalysis B: Environmental, 243 (2019) 502-512.
[38] X. Chen, Z. Zhang, L. Chi, A.K. Nair, W. Shangguan, Z. Jiang, Recent Advances in Visible-Light-Driven Photoelectrochemical Water Splitting: Catalyst Nanostructures and Reaction Systems, Nano-Micro Letters, 8 (2016) 1-12.
[39] F.E. Osterloh, Photocatalysis versus Photosynthesis: A Sensitivity Analysis of Devices for Solar Energy Conversion and Chemical Transformations, ACS Energy Letters, 2 (2017) 445-453.
[40] K. Takanabe, Photocatalytic Water Splitting: Quantitative Approaches toward Photocatalyst by Design, ACS Catalysis, 7 (2017) 8006-8022.
[41] X. Zhang, L.Z. Zhang, T.F. Xie, D.J. Wang, Low-Temperature Synthesis and High Visible-Light-Induced Photocatalytic Activity of BiOI/TiO2 Heterostructures, J. Phys. Chem. C, 113 (2009) 7371-7378.

[42] L. Kong, Z. Jiang, T. Xiao, L. Lu, M.O. Jones, P.P. Edwards, Exceptional visible-light-driven photocatalytic activity over BiOBr-$ZnFe_2O_4$ heterojunctions, Chem. Commun., 47 (2011) 5512-5514.
[43] Z. Jiang, F. Yang, G. Yang, L. Kong, M.O. Jones, T. Xiao, P.P. Edwards, The hydrothermal synthesis of BiOBr flakes for visible-light-responsive photocatalytic degradation of methyl orange, J. Photochem. Photobiol. A: Chem., 212 (2010) 8-13.
[44] L. Lu, L. Kong, Z. Jiang, H.H.-C. Lai, T. Xiao, P.P. Edwards, Visible-Light-Driven Photodegradation of Rhodamine B on Ag-Modified BiOBr, Catal. Lett., 142 (2012) 771-778.